Nano-scratch behavior of a bulk Zr–10Al–5Ti–17.9Cu–14.6Ni amorphous alloy

J.G. Wang,[a] B.W. Choi, and T.G. Nieh
Chemistry and Materials Science, Lawrence Livermore National Laboratory, P.O. Box 808, L-350, Livermore, California 94551-9900

C.T. Liu
Metals and Ceramics Division, Oak Ridge National Laboratory, P.O. Box 2008, Oak Ridge, Tennessee 37831-6376

(Received 27 August 1999; accepted 18 January 2000)

The tribological behavior of a Zr–10Al–5Ti–17.9Cu–14.6Ni (at.%) bulk amorphous alloy, in both the as-cast and annealed states, was investigated using nano-scratch tests, including ramping load scratch and multiple sliding wear techniques. The crystallization sequence of the alloy was also characterized. Mechanical properties, such as Young's modulus, hardness, friction coefficient, and tribological wear were measured. These properties were found to vary with microstructure. In general, an increase in annealing temperature results in an increase in hardness, which in turn produces a decrease in friction coefficient but an increase in wear resistance. Samples having a structure consisting of supercooled liquid matrix with dispersed nanocrystalline particles exhibit the best wear performance.

I. INTRODUCTION

Recently, a number of bulk amorphous alloys (BAAs) with critical cooling rates less than 10 K/s have been discovered in many muticomponent alloy systems of Ln–Al–TM,[1,2] Mg–Ln–TM,[3,4] Zr–Al–TM,[5,6] Zr–Ti–Al–TM,[7] Ti–Zr–TM,[8,9] Zr–Ti–TM–Be,[10] Pd–Cu–Ni–P,[11] and Fe–(Al, Ga)–(P, B, C, Si)[12,13] (where Ln = lanthanide metal and TM = transition metal). The high glass-forming ability of these alloys was observed to be dependent on the physical and chemical character of the constituent elements, as well as the number of elements in the alloys.[14–16] Amorphous alloys (or metallic glasses) have many unusual properties such as good corrosion resistance, high elasticity, and high hardness.[17,18] In view of their high hardness and strength, BAAs are promising materials for tribological (friction and wear) applications.

Several studies have been conducted on the wear and friction properties of rapidly quenched ribbons. The results, however, are controversial. Fe- Ni-, and Co-based amorphous alloys containing Si, B, and, sometimes, C, were used in these studies because of the consideration of using these alloys for magnetic recording devices.[19,20] Some metallic glasses showed high wear resistance, better than their crystallized counterpards.[21,22] However, opposite results have also been reported where metallic glasses exhibited wear performance well below expectation.[23–25] Some researchers demonstrated that an amorphous alloy containing a homogeneous dispersion of intermetallic compounds exhibited the best wear performance, and the fully amorphous material exhibited the highest wear rate.[26,27] The causes for these discrepancies are unclear. The purpose of this paper is to use nano-scratch tests to determine the tribological behavior of a Zr–10Al–5Ti–17.9Cu–14.6Ni (at.%) amorphous alloy and to shed light on the structure–property relationship.

II. EXPERIMENTAL PROCEDURES

A bulk amorphous alloy with a nominal composition of Zr–10Al–5Ti–17.9Cu–14.6Ni (at.%) was prepared by arc melting and drop casting, as described elsewhere.[28] The as-cast amorphous samples used for the test are of a cylindrical shape with a diameter of 7 mm. The amorphous nature of the cast samples was confirmed by using x-ray diffraction (XRD) and transmission electron microscopy (TEM). The sequential phase transition from glass to supercooled liquid and to crystallization states was studied by using differential scanning calorimetry (DSC) at a heating rate of 0.33 K/s.

To prepare samples for characterizing structures at different crystallization stages, and to minimize kinetic effects, various annealing treatments were performed *in*

[a] Address all correspondence to this author.
Present address: Department of Chemical and Biochemical Engineering and Materials Science, University of California, Irvine, 916 Engineering Tower, Irvine, California 92697-2575.
e-mail: wangjg@uci.edu

 © 2000 Materials Research Society

situ in the DSC cell with a heating rate of 0.33 K/s under flowing N_2. After reaching the desired temperature, the sample was rapidly cooled to room temperature. The heat-treated samples were examined using XRD and TEM.

Nanoindentation and nano-scratch tests were conducted on the as-cast and annealed samples using a Nano Indenter-XP®. Hardness and Young's modulus were measured using the continuous stiffness option, which yields hardness as a continuous function of depth into the sample.[29,30] A quartz sample was used as a standard for the initial calibration. Scratch tests were performed using the lateral force measurement option. A Berkovich indenter was used for the scratch test. The orientation of the indenter was aligned so that the sliding was performed with edge forward and face backward. Ramping load scratch tests were performed on samples over a 700-μm length. During a test, the applied normal load was linearly increased from an initial 20 μN to the maximum load, and the maximum loads selected in the present study were 20, 80, and 150 mN. Multiple sliding wear tests were also conducted. In each experiment, thirty-one passes were made over a 40-μm length using constant normal loads of 20 mN. The speed of the indenter for all sliding segments was about 1.0 μm/s.

III. EXPERIMENTAL RESULTS

A. Crystallization and mechanical properties

The DSC curve from the as-cast Zr–10Al–5Ti–17.9Cu–14.6Ni alloy (referred to hereafter as Zr–Al–Ti–Cu–Ni alloy) with a heating rate of 0.33 K/s is shown in Fig. 1. The amorphous alloy exhibits an endothermic reaction resulting from a glass transition, followed by the supercooled liquid region, and then an exothermic reaction caused by crystallization. The onset temperatures of the glass transition and crystallization, denoted by T_g and T_{x1} and T_{x2}, are determined to be 631, 729, and 818 K, respectively. From these measurements, three annealing temperatures, 683, 783, and 893 K, were selected; these temperatures correspond to the supercooled liquid region, and temperatures after the first and second crystallization peaks, respectively. The annealed samples were examined using XRD and the results are shown in Fig. 2, in which (a) is from the as-cast sample; (b), (c), and (d) are from samples annealed at 683, 783, and 893 K, respectively; and (e) is from a sample annealed at 923 K for 1 h. For discussion purposes, these five samples will be denoted as samples A, B, C, D, and E hereafter. According to a previous study,[31] the crystallization sequence of the amorphous Zr–10Al–5Ti–17.9Cu–14.6Ni alloy can be described by

$$\begin{aligned} \mathrm{Am} &\xrightarrow{683\ \mathrm{K}} \mathrm{Am}' \xrightarrow{783\ \mathrm{K}} \mathrm{Am}' + \mathrm{NiZr_2} + [\mathrm{Ni},\ (\mathrm{Zr},\ \mathrm{Ti})] \\ &\xrightarrow{893\ \mathrm{K}} \mathrm{Am}' + \mathrm{NiZr_2} + [\mathrm{Ni},\ (\mathrm{Zr},\ \mathrm{Ti})] + \mathrm{Zr(AlNi)_2} \\ &\quad + \mathrm{NiZr} \xrightarrow{923\ \mathrm{K},\ 1\ \mathrm{h}} \mathrm{Zr_2Cu} + \mathrm{NiZr_2} + \mathrm{Ni_{10}Zr_7} \\ &\quad + \mathrm{Al_3Zr_4} \quad , \end{aligned}$$

where Am and Am′ stand for the alloy in amorphous and relaxed states, respectively. A dark-field TEM image and selected-area electron diffraction pattern from samples A, B, C, D, and E are shown in Fig. 3. Both the as-cast and 683 K–annealed samples show a uniform amorphous structure [Figs. 3(a) and 3(b)]. The halo ring in the diffraction pattern of the 683 K–annealed sample is apparently sharper than that of the as-cast sample, as a result of the relaxation of the glassy state. In contrast, samples annealed at 783 and 893 K mainly consist of extremely fine Zr_2Ni grains with a size of less than 10 nm at 783 K and 40 nm at 893 K [Figs. 3(c) and 3(d)]. Diffraction patterns show distinct triple rings resulting from the three

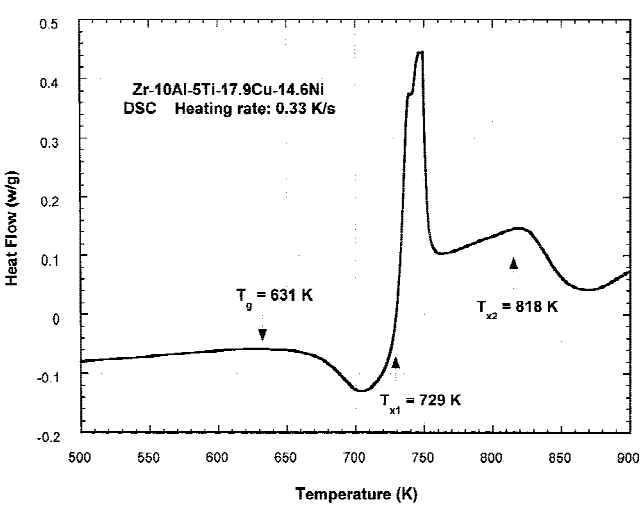

FIG. 1. DSC curve of the amorphous Zr–10Al–5Ti–17.9Cu–14.6Ni alloy with a heating rate of 0.33 K/s.

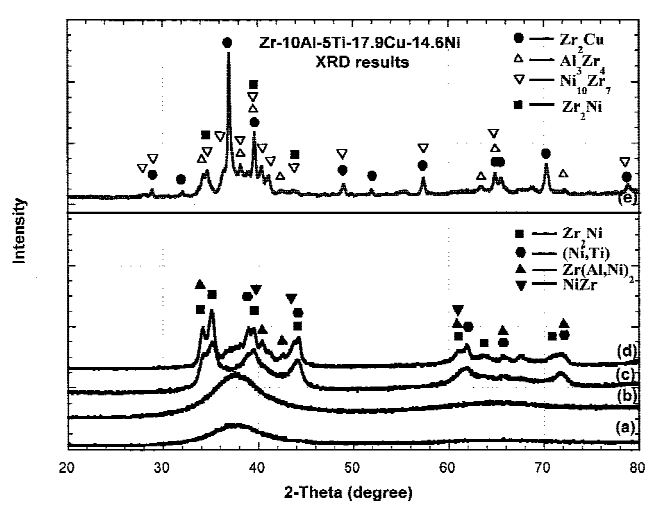

FIG. 2. XRD patterns from as-cast and annealed BAA samples: (a) as-cast, (b) 683 K, (c) 783 K, (d) 893 K, and (e) 923 K for 1 h.

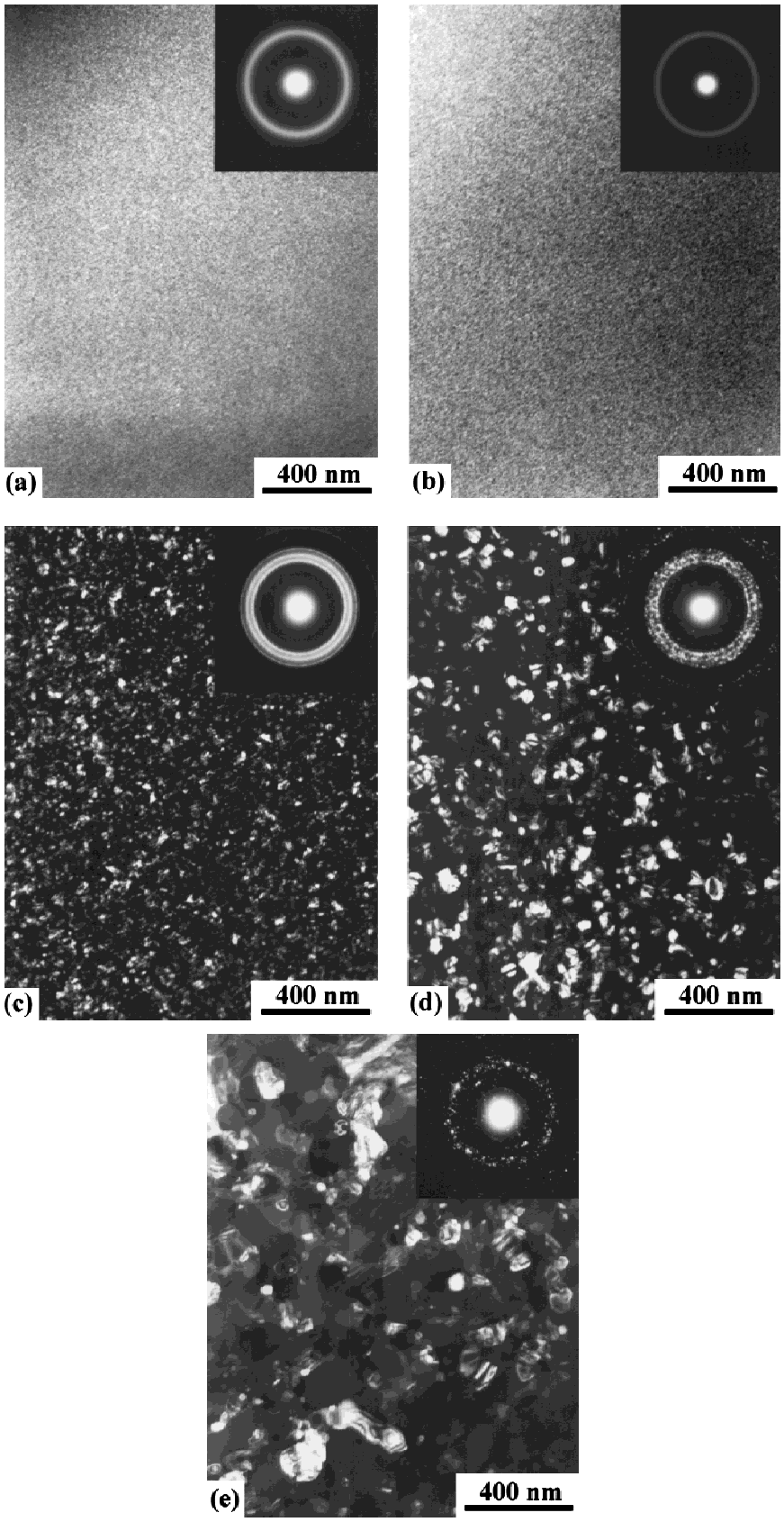

FIG. 3. Dark-field TEM images and selected-area electron diffraction patterns of the as-cast and annealed BAA samples: (a) as-cast, (b) 683 K, (c) 783 K, (d) 893 K, and (e) 923 K for 1 h.

diffraction peaks of the Zr_2Ni phase. The volume fraction of this nanocrystalline phase is estimated to be about 80% at 783 K and about 95% at 893 K. The structure of the sample annealed at 923 K for 1 h contains polycrystals with a mean grain size of about 250 nm, as shown in Fig. 3(e). The diffraction pattern consists of spotty reflection rings resulting from the presence of the Zr_2Cu phase; it no longer has the triple ring characteristic of the Zr_2Ni phase.

Hardness and Young's modulus measurements were performed on these samples. The results are summarized in Table I. It is readily observed that the as-cast sample has the lowest hardness and modulus values, while the fully crystallized sample exhibits the highest values.

B. Nano-scratch behavior

1. Ramping load scratch

A ramping load scratch (RLS) technique was used to characterize the friction behavior of the Zr–Al–Ti–Cu–Ni alloy. The measured friction coefficient [Figs. 4(a) and 4(c)] and surface profile [Figs. 4(b) and 4(d)] of samples A and B are shown in Fig. 4. The ramping normal load of 0.02–80 mN was used for the scratch tests. For the purpose of discussion, the ramping normal load is also included in the figure (bold solid line). As shown in Fig. 4, sudden increases in the friction coefficient (indicated by arrows) are frequently observed. It is interesting to note that this has also been often observed during nanoindentation of thin film. In the case of thin films, a sudden increase in friction coefficient is associated with microcracking or delamination of the films, which provides a measure of scratch resistance or adhesive strength of a film.[32–34] The load that causes the delamination is denoted as "critical load." In the case of bulk monolithic material, the sudden increase in friction coefficient is attributed to microcracking. Bulk amorphous alloys are known to be brittle; when the local strain exceeds the elastic limit during nanoindentation, microcracking is expected to occur.

TABLE I. Hardness and Young's modulus of as-cast and annealed Zr–10Al–5Ti–17.9Cu–14.6Ni alloy obtained by using different nanoindentation tests.

Sample	Test[a]	Depth (nm)	Load (mN)	Elastic modulus (GPa)	Hardness (GPa)
A: As-cast	HL	733 ± 4	60	112 ± 6	6.3 ± 0.6
	HD	2000	474 ± 4	92 ± 4	6.2 ± 2
B: 683 K annealed	HL	700 ± 3	60	119 ± 2	6.9 ± 0.1
	HD	2000	496 ± 8	100 ± 5	6.5 ± 0.2
C: 783 K annealed	HL	661 ± 3	60	118 ± 2	8.3 ± 0.1
	HD	2000	590 ± 12	99 ± 4	7.8 ± 0.2
D: 893 K annealed	HL	652 ± 4	60	119 ± 1	8.6 ± 0.1
	HD	2000	604 ± 10	99 ± 4	8.0 ± 0.2
E: 923 K annealed	HL	627 ± 4	60	150 ± 2	8.6 ± 0.2
(1 h)	HD	2000	619 ± 17	142 ± 1	8.3 ± 0.1

[a]HL, hardness test at a load; HD, hardness test as a depth.

As shown in Fig. 4(a), the baseline friction coefficient of sample A (i.e., as-cast sample) is about 0.2–0.25. However, at locations where sudden increases in friction coefficient occur, the friction coefficient can jump to about 0.3–0.35. (The scratch proceeds from left to right). To assess the scratch resistance of the sample, surface profiles [Fig. 4(b)] were measured by scanning the sample before and after the scratch test. It is noted that both the prescan and postscan were conducted using an extremely low load of 20 nN. The difference between the prescan and postscan profiles is presumably the damage caused by scratching, and the difference between the scratch and postscan profiles represents the elastic recovery of the sample. It is particularly pointed out that the locations where microcracking occurs (indicated by the sudden changes in friction coefficient) coincide with the depressions in the postscan surface profiles. The critical load can be determined from the first abrupt change in the surface profile and friction coefficient, and specifically it is about 28 mN (indicated in the figure). Other peaks at less than 28 mN on the friction coefficient profile may be caused by the surface roughness or break of the oxide layer during the initial stage of scratching. *In situ* optical microscopic observation revealed the formation of scratched debris at this load, confirming the occurrence of microcracking.

The structure of sample B (683 K annealed) is in a relaxed glass (supercooled liquid) state. The friction coefficient of this sample is averaged around 0.17 but it can sometimes jump to about 0.25–0.30. Sudden changes in friction coefficient are also observed at several locations, as indicated by arrows. The critical load determined by the first spike in both the surface and friction coefficient profiles [Figs. 4(c) and 4(d)] is about 46 mN, which is higher than that observed in sample A [Figs. 4(a) and 4(b)]. The higher critical load may be caused by the fact that a relaxed glass has less free volume, thus a stronger bonding and higher hardness value, than the as-cast glass. Gaskell[35] showed that when glass clusters approach the supercooled liquid state, the average chemical bonding increases.

For samples consisting of crystallized phases (samples C, D, and E), that is, samples annealed respectively at 783, 893, and 923 K, relatively low friction coefficients of about 0.15 were obtained; this is shown in Fig. 5. In contrast to samples A and B, virtually no "critical loads" were detected in these samples. The applied load appears to have no significant effect on the friction coefficient except in the initial scratch stage. Also, no evidence for the formation of debris was observed on the tested samples up to the maximum load of 80 mN. However,

when the maximum applied load was increased to 150 mN, critical loads of approximately 110 and 86 mN were observed in samples C and D, respectively. The baseline friction coefficient increases slightly to about 0.18 (Fig. 6) for both samples at this higher maximum load. The observed higher critical loads in samples C and D (both partially crystallized) are presumably associated with a less defective structure. It is worth noting that the critical load of 110 mN for the 783 K–annealed sample is higher than that for the 893 K–annealed sample (86 mN).

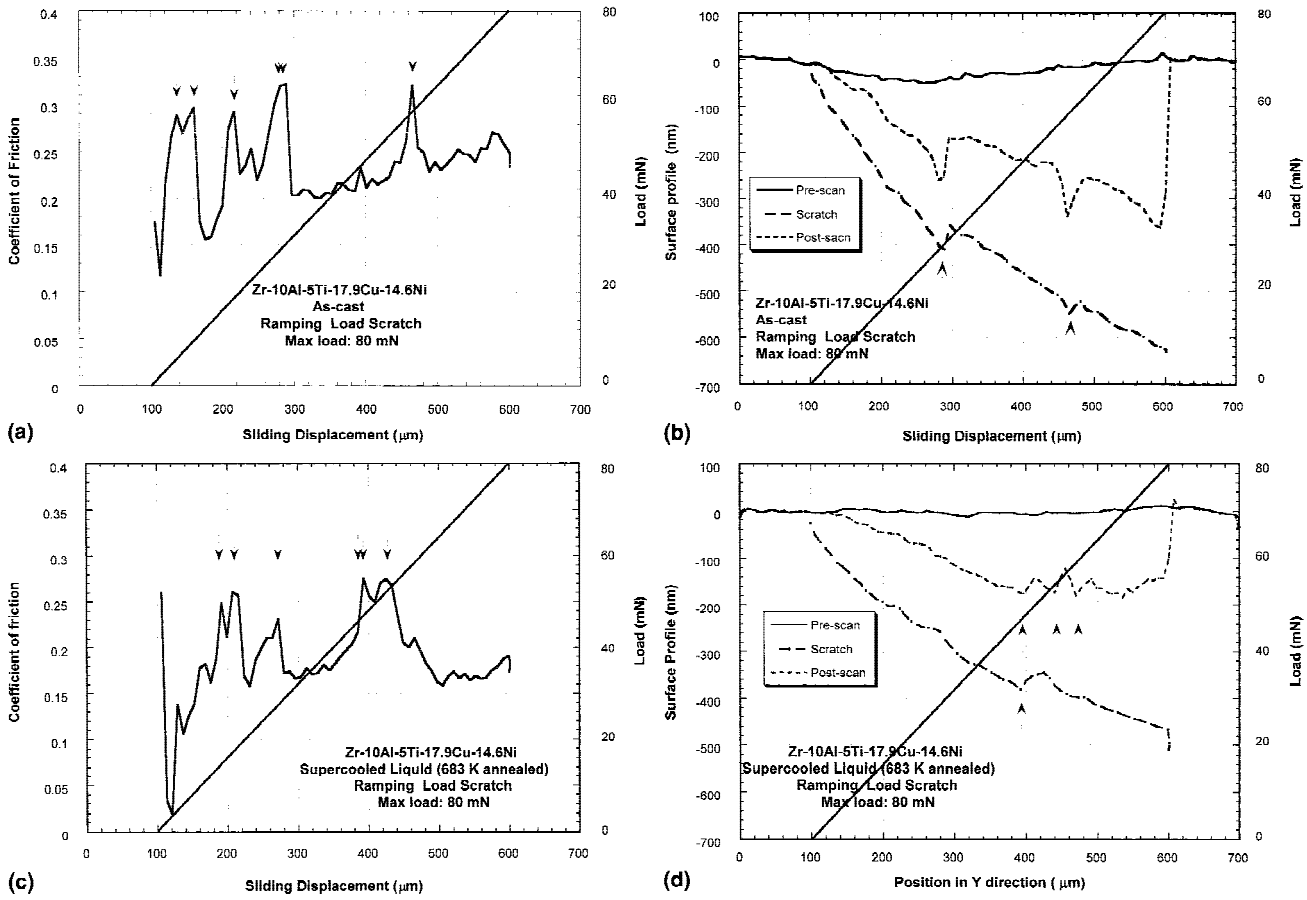

FIG. 4. Friction coefficient and surface profiles of the two samples in amorphous state (as-cast Am and supercooled Am′) scratched with ramping normal loads of 0.02–80 mN: (a) friction coefficient and (b) surface profile of as-cast Am; and (c) friction coefficient and (d) surface profile of supercooled Am′.

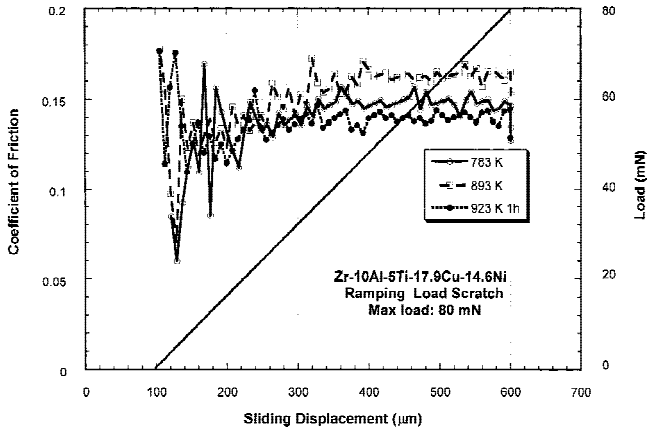

FIG. 5. Friction coefficient profiles of samples consisting of crystallized phases (annealed at 783 and 893 K, and at 923 K for 1 h) scratched with ramping normal loads of 0.02–80 mN.

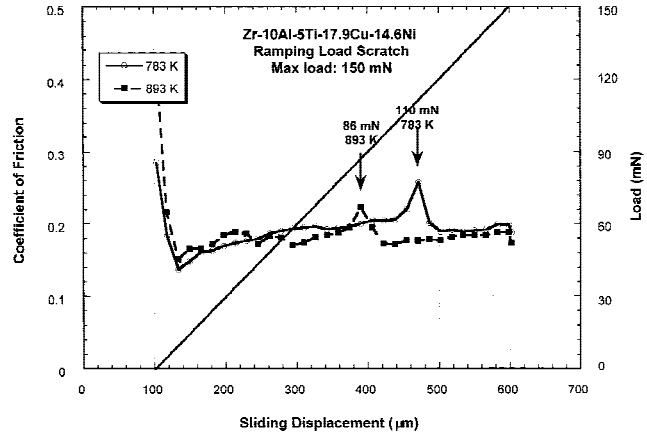

FIG. 6. Friction coefficient profiles of the nanocrystallized microstructure of the two samples (annealed at 783 and 893 K) scratched with ramping normal loads of 0.02–150 mN.

A summary of the baseline friction coefficients ($\overline{\mu}_B$), scratch (d_s), and postscan (d_p) depths at the maximum load of 80 mN for samples A, B, C, D, and E is listed in Table II. Data in the table are the average values from at least five tests. For each scratch experiment, at least five tests were performed to measure the critical loads. It is apparent that the as-cast sample has the highest friction coefficient, and the fully crystallized (nanocrystalline) sample has the lowest friction coefficient. Also, the friction coefficient decreases with increasing hardness, suggesting friction coefficient is dependent on the structure of the alloy.

The values of elatic recovery, represented by the difference between the scratch and postscan profile, $d_s - d_p$, for samples A, B, C, D, and E are 310, 350, 320, 320, and 220 nm, respectively. This result indicates that the allow in both the amorphous (A and B) and partially crystallized (C and D) states exhibits more elastic recovery than that in the fully crystallized state (E). However, the permanent damage caused by scratch is evaluated from the difference between the postscan and prescan profiles.

2. Multiple sliding wear

A multiple sliding wear (MSW) technique was also used for evaluating the wear resistance of Zr–Al–Ti–Cu–Ni alloy. The friction coefficients of the alloy in various annealed states are shown in Figs. 7(a)–7(e). It is noted in these figures that thirty-one sliding scans were made on each sample to ensure the attainment of a steady state. The applied normal load and sliding distance used were 20 mN and 40 μm, respectively. A constant normal load of 20 mN was intentionally chose to be lower than the critical load (28 mN) to avoid microcracking. Data displayed in Fig. 7 include both forward (odd number) and backward (even number) slides. Interestingly, despite the great difference between the edge-forward and face-backward alignment of the Berkovich diamond tip, friction behavior appears to be independent of the sliding direction (forward and backward). The friction coefficient (~0.1–0.2) was generally low in the initial scan, but increases rapidly to about 0.35–0.50 in the subsequent scans. It usually took more than five or six scans for the friction coefficient to reach a steady value.

The friction coefficient, μ, of sample A (as-cast) obtained in the first scan was only 0.15–0.2, increases rapidly, and reaches a steady state with an average value of about 0.42 [Fig. 7(a)]. In a similar manner, sample B (relaxed glass) also exhibits a low initial friction coefficient of about 0.1 and quickly reaches a steady state after five scans, yielding a slightly lower friction coefficient of about 0.34 [Fig. 7(b)]. It is also noted that the friction coefficient appears to increase slightly with sliding distance. A rapid increase in friction coefficient at the end of sliding, especially during the forward sliding, was apparently attributed to the pileup of worn material. As a result, the lateral forces tend to "lift" the indenter during sliding; this was described previously by Deng *et al.*[34]

The friction behavior of sample C (partially crystallized) is different from that of samples A and B. As shown in Fig. 7(c), the starting friction coefficient of sample C is low (~0.12), but increases rapidly to a peak value of about 0.28 after five scans. Instead of having a constant value, the friction coefficient gradually decreases to an average value of 0.24. This decrease may be attributed to work hardening taking place during multiple slides. Recalled that sample C has a microstructure containing nanocrystalline grains. Work hardening is expected to occur in crystalline grains and contribute to an increase in hardness, which, in turn, causes a decrease in friction coefficient. This is further supported by the results obtained from sample D. As shown in Fig. 7(d), a low final friction coefficient of about 0.15 is observed in sample D; this is because higher volume fraction of crystalline phase produces more work hardening. For the fully crystallized sample (sample E), the steady-state friction coefficient is about 0.3, which is higher than that for samples C and D (partially crystallized) but smaller than that for the amorphous samples.

The typical surface profiles of sample E before (prescan) and after (postscan) multiple sliding are shown in Fig. 8. The postscan depth can be used to estimate the wear resistance of a sample, because it represents the material that was worn away. The depth values are 600, 370, 250, 270, and 300 for samples A, B, C, D, and E, respectively. The steady-state friction coefficient for the forward sliding (μ_F), hardness (H), and postscan depth (d_p) under a normal sliding load of 20 mN are summarized in Table III. It is apparent in the table that there

TABLE II. Young's modulus, hardness, average value of friction coefficients ($\overline{\mu}_B$), scratch (d_s) and postscan (d_p) depths of a ramping load scratch test at the load limit of 80 mN.

Sample	Microstructure	E (GPa)	H (GPa)	$\overline{\mu}_B$	d_s (nm)	d_p (nm)
A: As-cast	Am	92–112	6.2–6.3	0.220	610	300
B: 683 K annealed	Am′	100–119	6.5–6.9	0.180	550	200
C: 783 K annealed	Am′ + $NiZr_2$ + [Ni, (Zr, Ti)]	99–118	7.8–8.3	0.155	460	140
D: 893 K annealed	Am′ + $NiZr_2$ + [Ni, (Zr, Ti)] + $Zr(AlNi)_2$ + NiZr	99–119	8.0–8.6	0.150	440	120
E: 923 K annealed (1 h)	Zr_2Cu + $NiZr_2$ + $Ni_{42}Zr_{58}$ + Al_3Zr_4	142–150	8.3–8.6	0.140	330	110

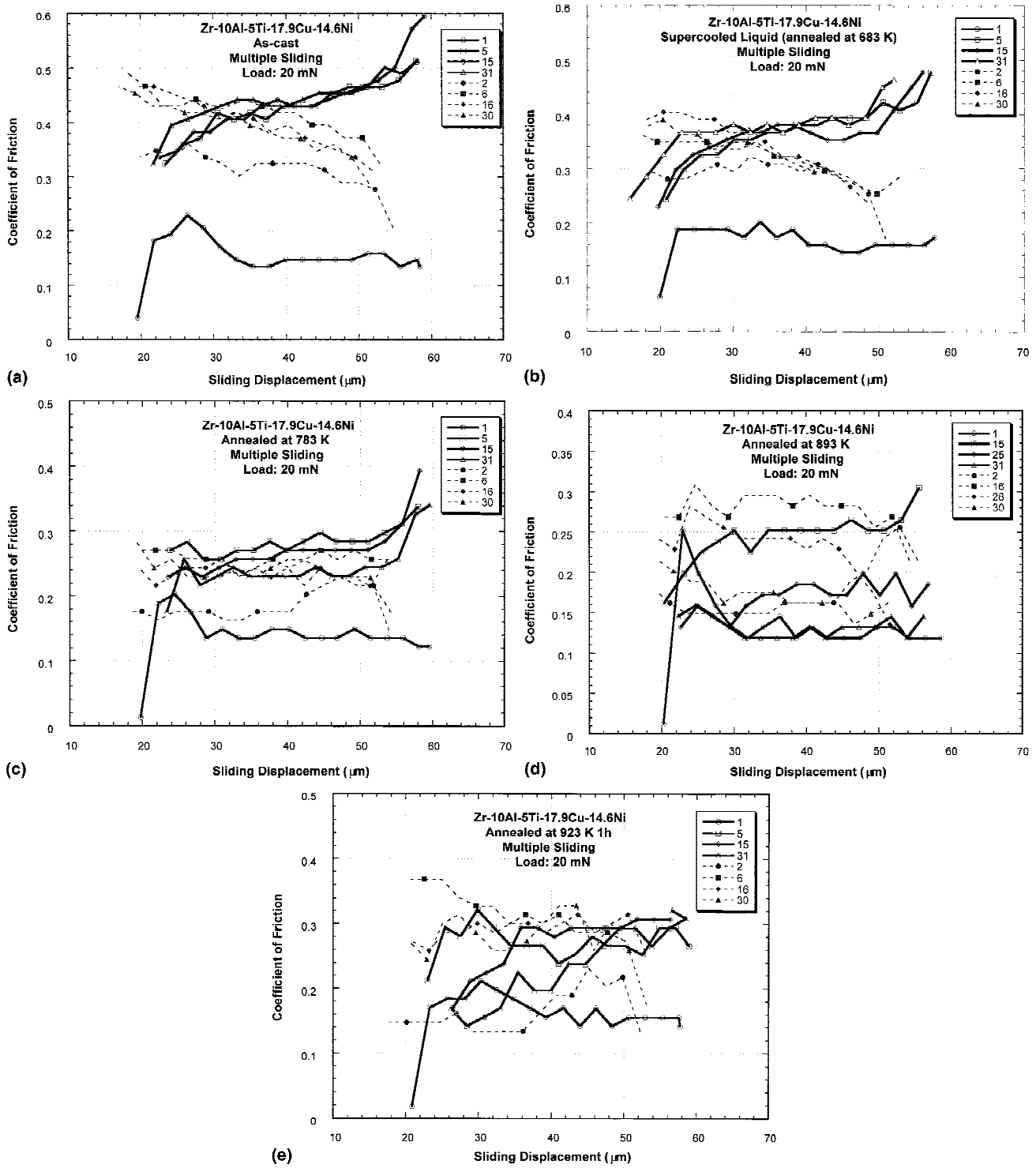

FIG. 7. Friction coefficient profiles of the multiple sliding wear test (thirty-one sliding scans) on all of the five samples under the normal load of 20 mN: (a) as-cast, (b) 683 K, (c) 783 K, (d) 893 K, and (e) 923 K for 1 h.

exists a general trend; namely, the worn depth is shallower for a harder sample. Once again, data indicate that both the partially crystallized (samples C and D) and fully crystallized (sample E) samples are more wear resistant than the as-cast sample (sample A).

IV. DISCUSSION

Friction is known to depend on a number of variables, such as chemical affinity between the two contacting materials, surface roughness, the presence or absence of

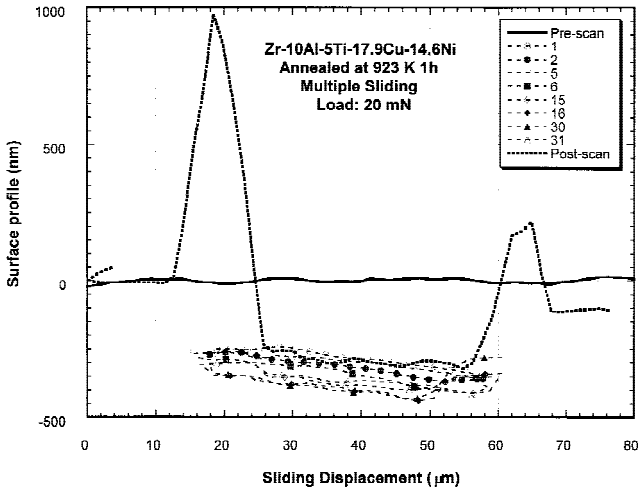

FIG. 8. Typical surface profiles of the multiple sliding wear test (thirty-one sliding scans) on sample E under the normal load of 20 mN.

oxides, absorbed films, and load conditions.[36] Existing data for the friction coefficient of metallic glasses cover a wide range; friction coefficients range from exceptionally low values (~0.015)[37] to medium values (0.2–0.6)[38,39] and to high values (0.8–1.0).[40–42] These data were obtained by using a spherical or cylindrical hard slider moving on sheet (tape or ribbon) metallic glass samples. Limited tribological data produced from ramping load scratch test using nanoindentation technique are available and they are summarized in Table IV. Results obtained in the present study are also included. It is noted in the table that critical loads exist in all materials, except the single-crystal Al and Al_2O_3–TiC. Also noted is the fact that the friction coefficient is slightly higher when the applied loading is above the critical load than when it is below the critical load.

Critical load can be considered as a measure of scratch resistance. As shown in Table IV, the present amorphous alloy apparently has a much higher critical load than the other materials, including ceramics. The critical loads of 110 and 86 mN found in samples C and D, respectively, are much higher than the 28 mN for the fully amorphous sample. This suggests that a material having a mixed amorphous–nanocrystalline microstructure is more scratch resistant than the fully amorphous sample. The postscan depth measurements from the MSW tests also confirmed that samples with an amorphous–nanocrystalline structure have the least wear loss; that is, the best wear resistance. Similar results have been observed in the study of the wear resistance of metallic glass ribbons[24–26] and Al-based bulk amorphous alloys.[27,43]

Kim *et al.*[44] recently demonstrated that a homogeneous dispersion of nanoscale crystalline particles embedded in Al-based amorphous matrix resulted in a significant increase in tensile strength, as compared to the corresponding single-phase, amorphous alloys. Similar results have also been reported in $Zr_{41}Ti_{13}Ni_{10}Cu_{13}Be_{23}$,[45] $Zr_{55}Al_{10}Ni_5Cu_{30}$,[46] and $Zr_{65}Al_{10}Ni_{10}Cu_{15}$[47] amorphous alloys. Apparently, a mixed amorphous–nanocrystalline structure offers high strength and hardness, and thus good wear resistance. This can be rationalized in the following way.

It is well-known that the Hall–Petch (HP) equation can describe the relationship between hardness (or yield strength) and grain size in conventional polycrystalline solids. The HP relation predicts that hardness should increase with decreasing grain size. The basic HP relation, given in Eq. (1), predicts that strength or hardness, H, should increase with decreasing grain size, d.

$$H = H_0 + Kd^{-1/2} \quad , \tag{1}$$

where H_0 if the intrinsic hardness and K is a material constant. Obviously, the equation has limitations because the strength cannot increase indefinitely with decreasing grain size, as shown in Fig. 9. From a practical viewpoint, for example, the strength value cannot exceed the theoretical strength; that is, the strength of a perfect whisker. Also, from another point of view, when the grain size approaches zero, the material essentially becomes amorphous. The grain boundary strengthening effect (HP relationship) will then disappear. There is some evidence indicating that the hardness (or strength) of an amorphous material is lower than its crystalline counterpart. For example, amorphous Al_2O_3 is softer than polycrystalline Al_2O_3,[48,49] and amorphous Si is softer than polycrystalline Si.[50] Thus, there must exist an optimum microstructure that yields the maximum hardness, as shown in Fig. 9. In the present study, it is a mixed amorphous–nanocrystalline structure that yields the maximum hardness. It is worth noting that the strength (or hardness) of a partially crystallized Zr–Al–Cu–Pd alloy was found to exhibit a maximum when the size of Zr_2(Cu, Pd) precipitate particles was ~10 nm and the volume fraction of the crystalline phase was about 75%.[51,52] This is consistent with the microstructures observed in samples C and D in the present study.

Data obtained in the present study indicate that there exists a general correlation between the hardness, friction coefficient, and wear resistance: a lower hardness produces a higher friction coefficient, and a higher friction results in a faster wear. The as-cast amorphous sample exhibits the lowest hardness and, thus, highest friction coefficient and poorest wear resistance. This result is consistent with the observations in some crystallized materials and metallic glass ribbons.[21,42] Comparing Tables II and III, it is noted that friction coefficient meas-

ured from the multiple sliding wear test is normally greater than that measured from the ramping load test. This is probably associated with the formation of a "transfer layer" on a scratched surface as suggested by Kishore *et al.*[17,53] In essence, a transfer layer produced during a slide can be removed by a subsequent slide at a load greater than the "critical load"; this results in a reduced friction coefficient. In the present study, increasing load was used during the ramping load tests. In contrast, the multiple sliding wear tests were always conducted at loads below the "critical load." However, it is pointed out that, despite the difference in the absolute value of friction coefficient, the general trend for these two measurements are consistent; namely, a higher hardness value leads to a lower friction coefficient.

V. CONCLUSIONS

Tribological (friction and wear) behavior of a bulk amorphous alloy Zr–10Al–5Ti–17.9Cu–14.6Ni (at.%), both in the as-cast and annealed states, was characterized by using ramping load scratch and multiple sliding wear tests. This study led to the following conclusions.

(1) The crystallization sequence of the alloy is described by

$$\begin{aligned} \mathrm{Am} &\xrightarrow{683\ \mathrm{K}} \mathrm{Am}' \xrightarrow{783\ \mathrm{K}} \mathrm{Am}' + \mathrm{NiZr_2} + [\mathrm{Ni, (Zr, Ti)}] \\ &\xrightarrow{893\ \mathrm{K}} \mathrm{Am}' + \mathrm{NiZr_2} + [\mathrm{Ni, (Zr, Ti)}] + \mathrm{Zr(AlNi)_2} \\ &\quad + \mathrm{NiZr} \xrightarrow{923\ \mathrm{K},\ 1\ \mathrm{h}} \mathrm{Zr_2Cu} + \mathrm{NiZr_2} + \mathrm{Ni_{42}Zr_{58}} \\ &\quad + \mathrm{Al_3Zr_4} \quad . \end{aligned}$$

(2) Both Young's modulus and hardness increase with increasing annealing temperature; the modulus and hardness values are, in the ascending order, amorphous, supercooled liquid, partially crystallized, and fully crystallized.

(3) Critical loads associated with microcracking were observed in all test samples. The as-cast material has the lowest critical load, and the critical load increases with increased annealing temperature.

(4) There exists a general correlation between the hardness, friction coefficient, and wear resistance; a lower hardness produces a higher friction coefficient and thus a faster wear.

(5) The present experimental results indicate that wear resistance is (in an ascending order): as-cast amorphous, supercooled liquid, fully crystallized, and

TABLE III. Steady-state friction coefficient for the forward sliding (μ_F) and postscan depth (d_p) under a normal sliding load of 20 mN in multiple sliding wear tests.

Sample	Microstructure	μ_F	H (GPa)	d_p (nm)
A: As-cast	Am	0.42	6.2–6.3	600 ± 20
B: 683 K annealed	Am′	0.30	6.5–6.9	370 ± 10
C: 783 K annealed	Am′ + $NiZr_2$ + [Ni, (Zr, Ti)]	0.25	7.8–8.3	250 ± 20
D: 893 K annealed	Am′ + $NiZr_2$ + [Ni, (Zr, Ti)] + $Zr(AlNi)_2$ + NiZr	0.15	8.0–8.6	270 ± 20
E: 923 K annealed (1 h)	Zr_2Cu + $NiZr_2$ + $Ni_{42}Zr_{58}$ + Al3Zr_4	0.27	8.3–8.6	300 ± 20

TABLE IV. Friction coefficient and critical load for several bulk materials measured from ramping load scratch test.

Material	Ramping load (mN)	Critical load (mN)	Friction coefficient	
			Baseline	Maximum
Single-crystal Si(100)	2–25	16	0.10	0.80
Ni–Zn ferrite	2–25	10	0.10	0.80
Al_2O_3–TiC	2–25	From beginning	0.15	0.30
SiC	2–25	15	0.12	0.75
Single-crystal Al	0.02–15	From beginning	0.35	0.50
A: As-cast	0.02–80	28	0.20	0.32
B: 683 K annealed	0.02–80	46	0.17	0.28
C: 783 K annealed	0.02–80	⋯	0.150	0.155
	0.02–150	110	0.18	0.28
D: 893 K annealed	0.02–80	⋯	0.150	0.15
	0.02–150	86	0.18	0.23
E: 923 K annealed (1 h)	0.02–80	⋯	0.14	0.14

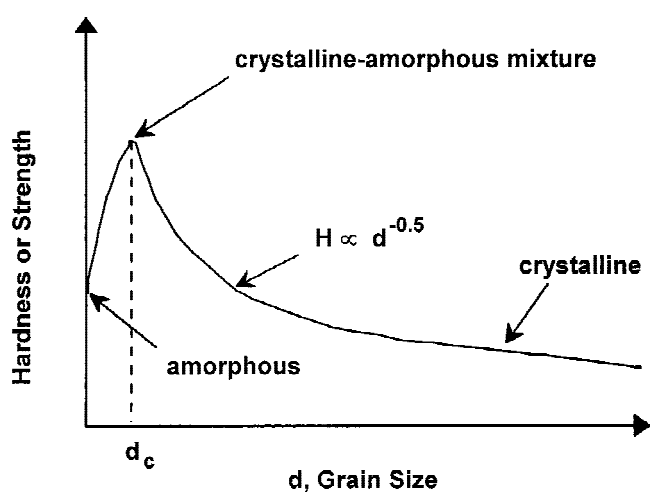

FIG. 9. Schematic illustration of Hall–Petch relationship for the metallic glass from amorphous to crystalline state.

amorphous–nanocrystalline mixture. Samples annealed at 783 and 893 K have a mixed amorphous–nanocrystalline structure and thus are the most wear resistant.

ACKNOWLEDGMENT

This work was performed under the auspices of the United States Department of Energy by Lawrence Livermore National Laboratory under Contract No. W-7405-Eng-48.

REFERENCES

1. A. Inoue, T. Zhang, and T. Masumoto, Mater. Trans., JIM **30,** 965 (1989).
2. A. Inoue, H. Yamaguchi, T. Zhang, and T. Masumoto, Mater. Trans., JIM **31,** 104 (1990).
3. A. Inoue, K. Ohtera, K. Kita, and T. Masumoto, Jpn. J. Appl. Phys. **27,** L2248 (1988).
4. S.G. Kim, A. Inoue, and T. Masumoto, Mater. Trans., JIM **31,** 929 (1990).
5. A. Inoue, T. Zhang, and T. Masumoto, Mater. Trans., JIM **31,** 177 (1990).
6. T. Zhang, A. Inoue, and T. Masumoto, Mater. Trans., JIM **32,** 1005 (1991).
7. A. Inoue, T. Shibata, and T. Zhang, Mater. Trans., JIM **36,** 1420 (1995).
8. A. Inoue, N. Nishiyama, K. Amiya, T. Zhang, and T. Masumoto, Mater. Lett. **19,** 131 (1994).
9. X.H. Lin and W.L. Johnson, J. Appl. Phys. **78,** 6514 (1995).
10. A. Peker and W.L. Johnson, Appl. Phys. Lett. **63,** 2342 (1993).
11. A. Inoue, N. Nishiyama, and T. Matsuda, Mater. Trans., JIM **37,** 181 (1996).
12. A. Inoue and J.S. Gook, Mater. Trans., JIM **36,** 1180 (1995).
13. A. Inoue and J.S. Gook, Mater. Trans. JIM **36** 1282 (1995).
14. A. Inoue, Mater. Trans., JIM **36,** 866 (1995).
15. A. Inoue, Mater. Sci. Eng. A **226–228,** 357 (1997).
16. A. Inoue, A. Takeuchi, and T. Zhang, Metall. Mater. Trans. A **29,** 1779 (1998).
17. U. Sudarsan, K. Chattopadhyay, and Kishore, in *Proceedings of the Fifth International Conference on Rapidly Quenched Metals,* edited by S. Steed and H. Warlimont (North-Holland, Amsterdam, The Netherlands, 1985), p. 1439.
18. A.L. Greer, Science **267,** 1947 (1995).
19. K. Ozawa, H. Walkasugi, and K. Tanaka, IEEE Trans. Magn. **20,** 425 (1984).
20. O. Kohmoto, K. Ohya, and T. Ojima, IEEE Trans. Magn. **25,** 4490 (1989).
21. D.G. Morris, in *Proceedings of the Fifth International Conference on Rapidly Quenched Metals,* edited by S. Steed and H. Warlimont (North-Holland, Amsterdam, The Netherlands, 1985), p. 1775.
22. N. Dolezal and G. Hausch, in *Proceedings of the Fifth International Conference on Rapidly Quenched Metals,* edited by S. Steed and H. Warlimont (North-Holland, Amsterdam, The Netherlands, 1985), p. 1767.
23. C. Atzeni, M. Pes, U. Sanna, A. Corrias, G. Paschina, and D. Zedda, Adv. Perform. Mater. **1,** 243 (1994).
24. K.L. Rutherford and I.M. Hutchings, J. Test. Eval. **25,** 250 (1997).
25. C.J. Wong and J.C.M. Li, Wear **98,** 45 (1984).
26. M. Anis, W.M. Rainforth, and H.A. Davies, Wear **172,** 135 (1994).
27. T. Gloriant and A.L. Greer, Nanostruct. Mater. **10,** 389 (1998).
28. C.T. Liu, L. Heatherly, D.S. Easton, C.A. Carmichael, J.H. Schneibel, C.H. Chen, J.L. Wright, M.H. Yoo, J.A. Horton, and A. Inoue, Metall. Mater. Trans. A **29,** 1811 (1998).
29. B.N. Lucas, W.C. Oliver, G.M. Pharr, and J-L. Loubet, in *Thin Films: Stresses and Mechanical Properties VI,* edited by W.W. Gerberich, H. Gao, J-E. Sundgren, and S.P. Baker (Materials Research Society, Pittsburgh, PA, 1997), p. 233.
30. W.C. Oliver and G.M. Pharr, J. Mater. Res. **7,** 1564 (1992).
31. J.G. Wang, B.W. Choi, T.G. Nieh, and C.T. Liu, J. Mater. Res. **15,** 798 (2000).
32. B. Bhushan, B.K. Gupta, and M.H. Azarian, Wear **181–183,** 743 (1995).
33. B.K. Gupta and B. Bhushan, Wear **190,** 110 (1995).
34. H. Deng, T.W. Scharf, and J.A. Barnard, IEEE Trans. Magn. **33,** 3151 (1997).
35. P.H. Gaskell, J. Non-Cryst. Solids **32,** 207 (1979).
36. J. Larsen-Basse, in *Friction, Lubrication, and Wear Technology,* edited by P.J. Blau (ASM International, The Materials Information Society, Materials Park, OH, 1995), p. 24.
37. J.K.A. Amuzu, J. Phys. D: Appl. Phys. **13,** L127 (1980).
38. D-H. Lee and J.E. Evetts, Acta Metall. **32**(7), 1035 (1984).
39. G. Girerd, P. Guiraldenq, and N. Du, Wear **102,** 233 (1985).
40. S.H. Whang and B.C. Giessen, in *Rapidly Solidified Amorphous and Crystalline Alloys,* edited by B.H. Kear, B.C. Giessen, and M. Cohen (New York, North-Holland, 1982), p. 301.
41. R. Klinger and H.G. Feller, Wear **86,** 287 (1983).
42. R. Moreton and J.K. Lancaster, J. Mater. Sci. Lett **4,** 133 (1985).
43. K. Ohtera, A. Inoue, T. Terabayashi, H. Nagahama, and T. Masumoto, Mater. Trans., JIM **33,** 775 (1992).
44. Y.H. Kim, A. Inoue, and T. Masumoto, Mater. Trans., JIM **31,** 747 (1990).
45. H.J. Fecht, Philos. Mag. B **76,** 495 (1997).
46. A. Inoue, Sci. Rep. RITU, **A42,** 1 (1996).
47. Y. Kawamura, H. Kato, A. Inoue, and T. Masumoto, Appl. Phys. Lett. **67,** 2008 (1995).
48. J-E. Sundgren and H.T.G. Hentzell, J. Vac. Sci. Technol., A **4,** 2259 (1986).
49. T.C. Chou, T.G. Nieh, S.D. McAdams, G.M. Pharr, and W.C. Oliver, J. Mater. Res. **7,** 2774 (1992).
50. G.M. Pharr, Rice University (private communication, 1998).
51. C. Fan and A. Inoue, Mater. Trans., JIM **38,** 1040 (1997).
52. C. Fan, A. Takeuchi, and A. Inoue, Mater. Trans., JIM **40,** 42 (1999).
53. Kishore, U. Sudarsan, N. Chandran, and K. Chattopadhyay, Acta Metall. **35,** 1463 (1987).